Journal of Physics: Conference Series

The Site and High Field βNMR Properties of $^{8}Li^{+}$ Implanted in α-Al_2O_3

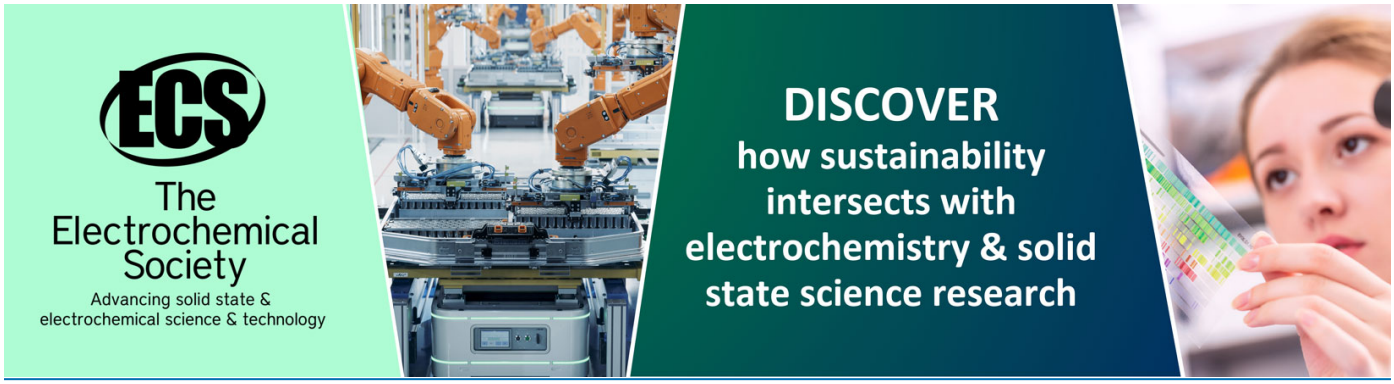

Journal of Physics: Conference Series **2462** (2023) 012009 doi:10.1088/1742-6596/2462/1/012009

The Site and High Field βNMR Properties of $^8Li^+$ Implanted in α-Al_2O_3

W.A. MacFarlane[1,2,3,*], J.K. Shenton[4,*], Z. Salman[5], A. Chatzichristos[2,6,7], D.L. Cortie[8], M. Dehn[2,6], D. Fujimoto[2,3,6], V.L. Karner[1,2,3], R.F. Kiefl[2,3,6], D. Koumoulis[9], C.D.P. Levy[3], R.M.L. McFadden[1,2,3], I. McKenzie[3,10,11], G.D. Morris[3], M.R. Pearson[3], M. Stachura[3], J.O. Ticknor[1,2]

[1] Chemistry Department, University of British Columbia, Vancouver, BC, V6T 1Z1, Canada
[2] Stewart Blusson Quantum Matter Institute, University of British Columbia, Vancouver, BC, V6T 1Z1, Canada
[3] TRIUMF, Vancouver, BC, V6T 2A3 Canada
[4] Scientific Computing Department, Science & Technology Facilities Council, Rutherford Appleton Laboratory, Didcot OX11 0QX, United Kingdom
[5] Laboratory for Muon Spin Spectroscopy, Paul Scherrer Institute, CH-5232 Villigen PSI, Switzerland
[6] Department of Physics and Astronomy, University of British Columbia, Vancouver, BC, V6T 1Z1, Canada
[7] Physics Department, Khalifa University, United Arab Emirates
[8] Australian Nuclear Science and Technology Organisation, Lucas Heights, New South Wales 2234, Australia
[9] Center for Applied Energy Research, University of Kentucky, Lexington, KY 40511, USA
[10] Department of Chemistry, Simon Fraser University, Burnaby, BC, V5A 1S6, Canada
[11] Department of Physics and Astronomy, University of Waterloo, Waterloo, Ontario, N2L 3G1, Canada
[*] contributed equally to this work

E-mail: wam@chem.ubc.ca

Abstract. We present high (> 2 T) magnetic field βNMR measurements of $^8Li^+$ implanted in single crystals of sapphire, a commonly used backing material for other samples. From the well-resolved quadrupolar splitting, we extract the electric field gradient (EFG) at the implanted $^8Li^+$ site. Comparison with supercell density functional theory calculations of the EFG allows us to identify the octahedral interstitial site as the most likely candidate. In contrast to the zero field βNQR spectra, where multiple singals are detected, only a single site is evident at high field. We discuss possible explanations for this discrepancy. The spin lattice relaxation is extremely slow ($1/T_1 < 0.02$ s^{-1}) over a broad temperature range from 4 to 300 K, demonstrating that cross relaxation with the ^{27}Al nuclear spins is quenched in such high magnetic fields.

1. Introduction

Sapphire, corundum structured α-Al_2O_3, is a robust, highly thermally conductive, ultrahigh vacuum compatible binary oxide commonly used as a film substrate or backing material (onto which smaller samples are mounted) for ion-implanted βNMR. As such, it presents an important potential background from spilled beam, or for a thin film, in the case the implanted

ion penetrates the film and stops in the substrate (see the example of polystyrene films in these proceedings). It is also a (very) wide band gap transparent host for various optically active impurities such as Cr^{3+} and Nd^{3+}[1] that are the basis for its use as a laser medium. Other defects also have interesting optical properties[2, 3], including applications in radiation dosimetry[4]. We demonstrated that its related *ionoluminescence*[5, 6] is useful for ^{8}Li beamspot imaging[7]. As a substrate for film deposition, its crystalline surfaces are also well-studied[8]. Here we report the NMR behaviour at high (Tesla) fields applied along the hexagonal c axis. This data presents an important test case for site determination of the implanted $^8Li^+$ that may be directly useful in interpreting βNMR data in the isostructural magnetic oxides Cr_2O_3 and Fe_2O_3[9] and also further the general approach to site determination enabled by calculations. We report supercell DFT calculations of the EFG at several candidate Li sites in α-Al_2O_3, allowing us to identify the site.

2. Experiment

βNMR experiments were carried out at the Isotope Separator and Accelerator (ISAC) facility at TRIUMF between 2005 and 2021. The ^{8}Li has nuclear spin $I = 2$, radioactive lifetime $\tau = 1.21$ s, gyromagnetic ratio $\gamma = 6.3015$ MHz/T, and a small electric quadrupole moment $Q = +32.6$ mb. A highly polarized beam of $^8Li^+$ was implanted in the sample with a typical flux of 10^7/s into a beam spot ~ 2 mm in diameter. The nuclear polarization was monitored through the anisotropic β-decay in two fast plastic scintillation detectors up- (B) and down- (F) stream of the sample. Resonances were measured with a continuous beam by introducing a transverse CW RF magnetic field B_1, and scanning its frequency through $\nu_0 = \gamma B_0/(2\pi)$ at a rate slow compared to τ. On resonance, the $^8Li^+$ precesses about B_1, and the β-decay asymmetry is reduced. To measure the spin lattice relaxation, the incoming $^8Li^+$ beam was pulsed with a fast electrostatic kicker, and the relaxation of the beta decay asymmetry was monitored during and after the beam pulse with no RF field applied. In each type of measurement both spin directions of the $^8Li^+$ (parallel and antiparallel) relative to the large static field B_0, produced by a high homogeneity superconducting solenoid, were collected by alternating the helicity of the polarizing laser light. This has a number of advantages, including determination of the baseline (zero of asymmetry). The field B_0 ranged from 2.2 to 6.55 T perpendicular to the surface. The samples were commercial α-Al_2O_3 wafers 0.5 mm thick with surface normal oriented within 0.5° of the (0001) c crystal axis. The surface was highly polished ("epi-ready") having an RMS roughness less than 1 nm.

To describe the NMR splitting, we use the conventionally defined quadrupole frequency[10, 11]

$$\nu_Q = \frac{3}{2I(2I-1)}\left[\frac{e^2qQ}{h}\right] = \frac{1}{4}\left[\frac{e^2qQ}{h}\right] = \frac{C_Q}{4},$$

where C_Q is the nuclear quadrupole coupling constant. From the orientation dependence of the zero field asymmetry[7], the principal axis of the electric field gradient (EFG) tensor eq is along the c axis. Here with the applied $B_0 \parallel c$, the first order satellites are at[10]

$$\nu_0 + n\frac{\nu_Q}{2}, \tag{1}$$

where $n = \pm 3, \pm 1$. With this definition, the zero field NQR frequencies are $\nu_{\rm NQR} = 3\nu_Q/2$ and $\nu_Q/2$.

3. Calculations

In order to determine the $^8Li^+$ stopping site(s), we carried out density functional theory (DFT) calculations using the plane-wave DFT code CASTEP[13, 14, 15]. We used ultrasoft

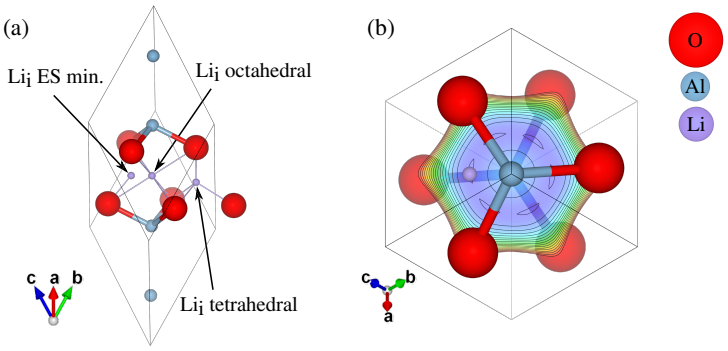

Figure 1. The initial Li^+ (purple) interstitial starting configurations in the rhombohedral unit cell of α-Al_2O_3 with O (red) and Al (blue). (a) The octahedral, tetrahedral and electrostatic minimum (ES min.) Li^+ sites. (b) Li^+ at the 6 fold degenerate electrostatic potential minimum site (purple) that is relevant for the μ^+ in Cr_2O_3[12]. Contours show the electrostatic potential surrounded by 6 oxide anions and more distant Al. The octahedral site is at the centre of the doughnut shaped potential minimum.

pseudopotentials[1] and the PBEsol[16] exchange-correlation functional. In combination with a plane-wave cut-off of 900 eV and a k-point spacing of 0.045 $Å^{-1}$, this strategy adequately captures the crystal structure of α-Al_2O_3. Using these parameters we predict a rhombohedral lattice constant of 5.138 Å and rhombohedral angle of 55.34°, both within 0.2% of the 120 K experimental X-Ray structure[17]. The method for calculating EFG tensors is outlined in Ref.[14]. To further assess the reliability of the calculations, the same code and crystal structure was used to calculate C_Q for stable ^{27}Al in pure α-Al_2O_3, yielding 2.305 MHz, in very good agreement with a recent experimental determination of 2.30(4) MHz[18]. Additional validation of the computational setup including the choice of the exchange-correlation functional and the numerical parameters can be found in the Supplemental Material (SM) [19].

Because of the extremely low flux, the implanted ^{8}Li constitutes an ideally dilute limit impurity. In a crystalline host, the implanted ion typically adopts a high symmetry site. For non-cubic sites, this is reflected by a well-defined quadrupole splitting. In most cases, the lowest energy site is populated, but, particularly at low temperature, other metastable sites may be observed.

To search for $^8Li^+$ stopping site(s), we constructed a $3 \times 3 \times 3$ supercell of PBEsol-relaxed α-Al_2O_3, added in a single $^8Li^+$ ion (with a compensating uniform background charge) at an interstitial position and fully relaxed the positions of all the ions. We did this for three candidate interstitial positions: the octahedral (Wyckoff $6b$), tetrahedral ($36f$) and the electrostatic minimum sites, see Figure 1a). The electrostatic minimum (see Figure 1b)) is one of six equivalent sites lying on a doughnut-shaped potential around the octahedral site, see the discussion of muon sites in Cr_2O_3[12]. Though the concentration of Li in the periodic calculation (0.019 per Al_2O_3) is vastly larger than the experiment, the supercell is large enough to provide a reasonable estimate for the dilute limit. We compared the calculated C_Q for a fully-relaxed $^8Li^+$ ion (in the octahedral site) in a $2 \times 2 \times 2$ supercell and a $3 \times 3 \times 3$ supercell shown in Figure 2b) and found just a 0.2% difference.

[1] The pseudopotentials were generated on-the-fly and are defined by: Li:1|1.0|14|16|18|10U : 20(qc = 7), O:2|1.1|17|20|23|20 : 21(qc = 8) and Al:3|2.2|2.2|1.4|4|5|5|30 : 31 : 32U2U2.

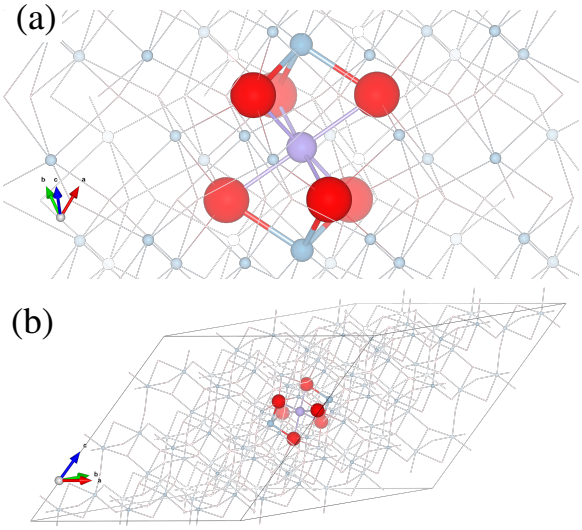

Figure 2. The geometry-optimised structure of a $3 \times 3 \times 3$ supercell of α-Al_2O_3 with a Li^+ (purple) defect at the octahedral interstitial site, showing (a) a close-up of the local structure around the defect and (b) the full simulation cell. Al ions are shown in blue and the nearest-neighbour oxide ions are shown in red. Nearest neighbour Al ions are highlighted with larger spheres.

In addition to interstitial sites, we also studied the isolated substitutional sites by initiating the $^8Li^+$ ion in O and Al vacancies with different charge states as indicated in Table 1. For the oxygen vacancy site, the $^8Li^+$ ion relaxed nearly to the octahedral interstitial with an O vacancy nearby; i.e. we obtained a Li_i-V_O complex configuration. The $^8Li^+$ in the Al vacancy, by contrast, remained in the Al site with minimal displacement; i.e. it forms a (meta-)stable substitutional Li_{Al} defect. In Table 1, we summarize the calculated EFG tensors for the relaxed configurations, and compare them to the experimental results below.

Further details of the DFT calculations and computational setup, including the structures we obtained, can be found in the SM[19].

4. Results and Discussion

The NMR of $^8Li^+$ implanted into α-Al_2O_3 consists of a quadrupole multiplet of 4 satellite lines, such as the one shown in Figure 3, corresponding to the $|\Delta m| = 1$ transitions among the $2I + 1 = 5$ magnetic sublevels. The optically hyperpolarized initial state of the ^8Li spin causes the relative intensity of the outer satellites ($m = \pm 2 \leftrightarrow \pm 1$ transitions) to be larger than the inner ($m = \pm 1 \leftrightarrow 0$) ones, in contrast to conventional NMR, and, as seen in the data, opposite satellites $\pm n$ are evident in spectra with opposite ^8Li polarization. To extract the quadrupolar frequency, the spectra were fit to a sum of 4 Lorentzians with common widths and positions determined by the two parameters of Section 2. The fit also included a small (unsplit) resonance near the Larmor frequency which is likely a background. The fits determine ν_Q with considerable accuracy and the results are shown as a function of temperature in Figure 4. Its magnitude is

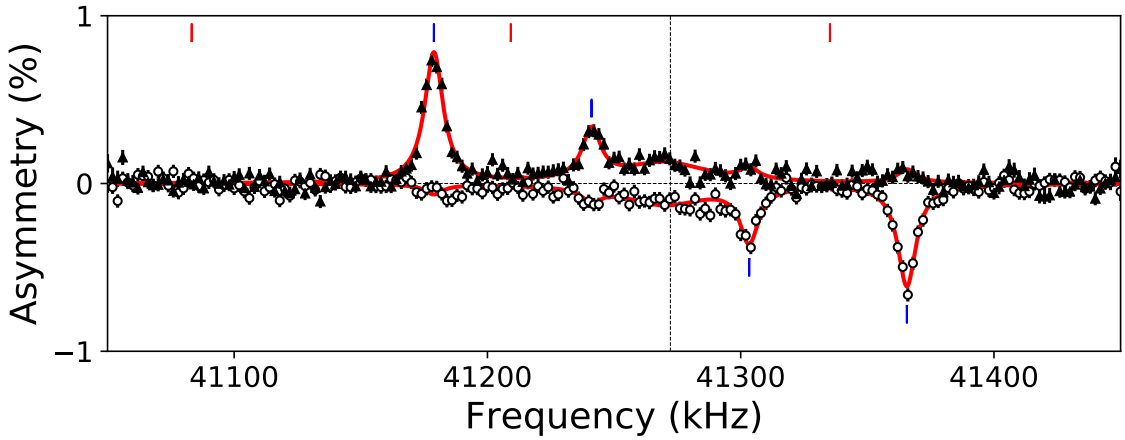

Figure 3. The βNMR spectra of $^8Li^+$ implanted at 20 keV into α-Al_2O_3 at 6.55 T $\parallel c$ and 300K with the helicity (anti)parallel to the field (triangles) open circles. The resonances marked with the blue ticks comprise a single multiplet with $\nu_Q = 62.252$ kHz, consistent with the lower frequency NQR[7]. The red ticks mark the positions expected for the first order satellites ($\theta = 0$) and ν_Q corresponding to the higher frequency NQR. There is an additional small broad line near the Larmor frequency marked by the vertical dashed line.

intermediate between the small values seen in Sr_2RuO_4[20] and ZnO[21] and the very large values in the perovskite oxides[22, 23]. As in other cases[21], ν_Q decreases with temperature. Primarily this is a consequence of thermal population of phonons[24]. Although the data are sparse, we fit $\nu_Q(T)$ to the common phenomenological form $\nu_{Q0}(1 - cT^{1.5})$ shown as the dotted line in Figure 4, with parameters $\nu_{Q0} = 63.28(14)$ kHz and $c = 3.2(5) \times 10^{-6}$ kHz/K$^{1.5}$.

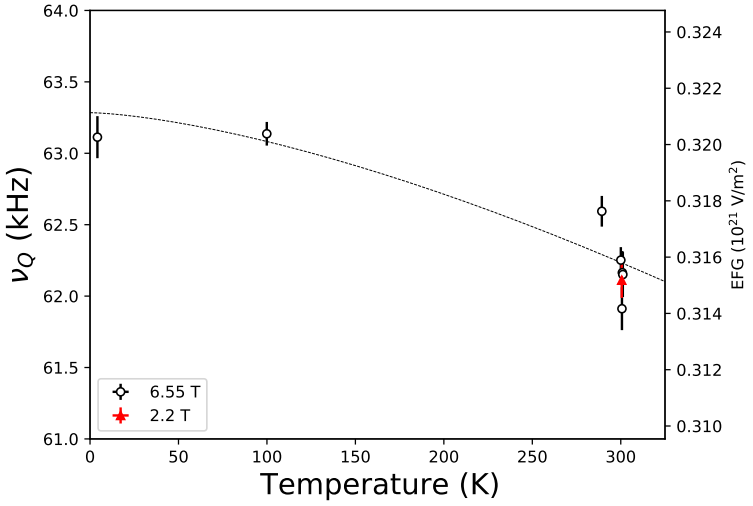

Figure 4. The measured quadrupole frequency of $^8Li^+$ in α-Al_2O_3 as a function of temperature at 6.55 T ($\parallel c$) is consistent with the value at 2.2 T (red triangle).

The high field spectra such as Figure 3 are consistent with a single high symmetry crystallographic site with a well-defined EFG for the implanted $^8Li^+$. However, previously

we observed two distinct βNQR resonances[7] and concluded there were two sites. The lower frequency NQR is consistent with the quadrupole splitting in Figure 3, i.e. $\nu_{\rm NQR} \sim 93$ kHz. If we assume that the higher frequency NQR corresponds to another axial site, we should observe a second quartet with 3 of the satellite positions marked by the red ticks in Figure 3. (The fourth is offscale to the right beyond the range of the scan.) Clearly, such a quartet is absent.

What might account for the second NQR? In some cases, we observe double quantum $|\Delta m| = 2$ transitions in high field spectra[25]. In the NQR, a $|\Delta m| = 2$ transition requires an energy $h(3\nu_Q/2 + \nu_Q/2) = 2h\nu_Q$, i.e. two RF photons of frequency ν_Q, lower than $\nu_{\rm NQR}$, but the high frequency NQR is observed at $\sim$ 186 kHz, very close to *twice* the lower one. Nonlinearity of the NQR power amplifier could lead to odd harmonics in the RF irradiation, but not the required even multiple of two.

On the other hand, if the high frequency NQR does represent a second site, one must explain the absence of the corresponding satellites in spectra such as Figure 3. The high frequency NQR is considerably smaller and broader[7], so if the corresponding satellites are further broadened in high field, they may be unobservable with the limited amplitude B_1. This might occur if the EFG is not perfectly aligned with c, or if the corresponding defect site is paramagnetic with a bound unpaired electron spin (e.g. an oxygen hole[26]) in the vicinity. Preliminary DFT calculations suggest a self-trapped hole polaron on a nearest neighbour oxide ion has a hyperfine interaction with the nearby ^{8}Li$^+$. This may help to explain the lack of a corresponding high field signal, since a small hyperfine splitting would produce substanially more broadening in high field (than at zero field). Radiation damage is known to produce paramagnetic defects in sapphire. The primary EPR signal is attributed to the F^+ color center with an electron trapped at an oxygen vacancy[27]. However, there is no missing amplitude evident in high field (see below), so if there is a paramagnetic fraction, it is not fast relaxing.

While the second NQR remains puzzling, we can proceed to compare the observed ν_Q with the calculations. The calculated EFG tensors are presented in Table 1 for the relaxed configurations. The CASTEP output files containing the relaxed structures and full EFG tensors for each configuration can be found in the SM[19]. Of the interstitial configurations explored, only the octahedral site is found to be stable - the electrostatic-minimum and tetrahedral interstitial configurations both relaxed into the octahedral configuration, Li$_i$. The ^{8}Li$^+$ ion causes a local structural distortion around the octahedral site; most significantly, it pushes the two nearest neighbour Al ions away, each by 0.22 Å, along the c axis. A recent study of H$^+$ interstitials in α-Al$_2$O$_3$[28] also found the octahedral site to be the only stable interstitial configuration. For Er^{3+} ions implanted into α-Al$_2$O$_3$, 70% were found to occupy octahedral interstitial site, albeit one that is displaced slightly from the ideal octahedral position[29]. Another 20% of the Er^{3+} ions were found to occupy the tetrahedral site. We were unable to stabilise the tetrahedral site for ^{8}Li$^+$ions, despite several initial configurations and constraints. It may be that the larger ionic radius [30] of Er^{3+} (0.89 Å) relative to Li^{1+} (0.76) could explain the different behaviour.

Zero-point motion contributions have been considered at the octahedral site. Specifically, we computed the quantum averaged ν_Q for ^{8}Li$^+$ around the minimum, following the method in Ref. [31]. We find that the quantum-averaged ν_Q is about 2% lower than the value computed at the minimum, bringing it in slightly closer agreement with experiment. Crucially, no other minima were found in this way.

The octahedral configuration has a predicted EFG in reasonable agreement with the observed ν_Q, but the remaining discrepancy ($\sim$ 12%) is substantially larger than for the ^{27}Al in pure α-Al$_2$O$_3$ (without Li). DFT predictions of EFG tensors commonly overestimate the experimental values[32] with a lattice dynamic reduction being the primary candidate for the lower experimental ν_Q. Naturally, the calculated EFG is also sensitive to the lattice constant. For these estimates we used the PBEsol prediction (5.1387 Å) which agrees well with the 120 K value (5.1294 Å) from X-Ray diffraction[17]. We find that the predicted ν_Q scales linearly with the

lattice parameter (with a larger lattice constant leading to a smaller EFG) when we uniformly scale the simulation cell and relax the internal coordinates. The experimental ν_{Q0} would be obtained using a lattice constant of 5.2569 Å (2.3% larger than the PBEsol prediction). Given that the lattice constant obtained using the PBEsol functional is in good agreement with the low-temperature experimental value, and that we find that the supercell size is well-converged (see section Section 3), this discrepancy may be attributed to lattice dynamic effects[24] or to the effect of the exchange-correlation functional approximation on the defect-induced local distortions.

In addition to the simple isolated defect structures above, we studied several potential complexes. In the process of slowing down, the implanting $^8Li^+$ will knock host ions of out of their regular lattice sites producing Frenkel (vacancy-interstitial) pairs. The threshold energy for this process is on the order of 50 eV[33], so near the end of its track, the $^8Li^+$ creates a final pair and then continues some distance before stopping. If it stops in the immediate vicinity of a Frenkel pair, the local lattice symmetry is lowered, and this will be reflected in the EFG. Moreover, because there is a distribution of such environments, depending on the distance vectors between the stopped ^{8}Li and the interstitial and vacancy, there is a distribution of EFGs, and this will produce a quadrupolar broadening. In many cases, we see very narrow lines, indicating that ^{8}Li is isolated (sufficiently distant) from any such defects, so that their effects are negligible. However, in some cases, we see a broad line (particularly at low temperature) that may reflect such "disorded" sites. If the stopped $^8Li^+$ is near such a defect, it may be attracted to it and bind into a defect complex with the vacancy, the interstitial or both. Indeed, the vacancy required for the isolated substitutional site would almost certainly be implantation-related (rather than thermodynamic). We assess the effects of nearby defects and the potential for complexation using DFT calculations in the following.

Introducing an O vacancy in the vicinity of the $^8Li^+$ reduces the calculated ν_Q slightly, depending on the charge state of the vacancy. This however, also induces anisotropy in the calculated EFG tensor. The $^8Li^+$ EFG principal axis no longer lies precisely along the hexagonal c-axis when an O vacancy is in the vicinity.

The $^8Li^+$ could also occupy, in principle, an Al vacancy with a calculated ν_Q of 16.35 kHz, though this is well below the experimental ν_Q. In the case of a cation Frenkel-like pair (i.e. an Al ion in the octahedral interstitial site and the $^8Li^+$ ion in the Al vacancy), the calculated EFG tensor is almost identical to that for the $^8Li^+$ interstitial site. The geometry-optimised local structure of $^8Li^+$ in the Frenkel pair is nearly identical to that of the $^8Li^+$ interstitial site which could account for the similar EFG tensors.

Table 1. Calculated ν_Q for specific Li defect configurations using the PBEsol-predicted lattice parameters, see text for details.

Site	Charge (e)	ν_Q (kHz)	Principal Axes	η
Li_i	+1	70.90	(0.000, 0.000, 1.000)	0.00
Li_{Al}, Al_i	+1	70.70	(0.000, 0.000, 1.000)	0.00
Li_{Al}	-2	16.35	(0.000, 0.000, 1.000)	0.00
Li_i-V_O	+1	68.58	(-0.002, 0.002, 1.000)	0.05
Li_i-V_O	+3	63.93	(0.292, 0.039, 0.956)	0.54

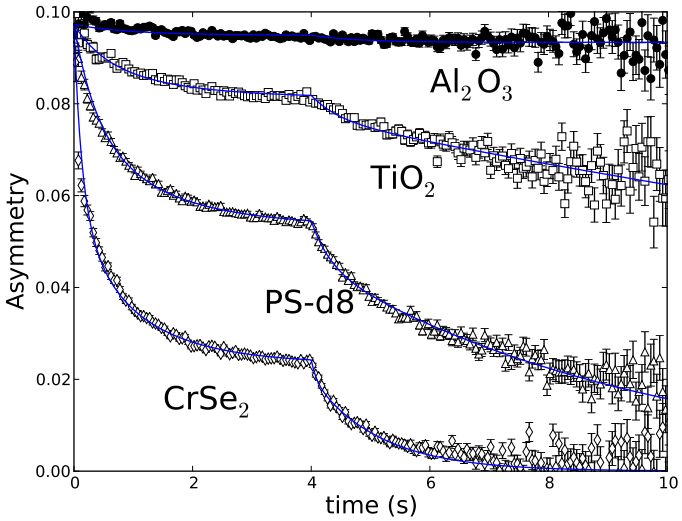

Figure 5. Spin lattice relaxation data at room temperature and 6.55 T in a variety of materials (see text for details). The relaxation function is convoluted with the 4 second beam pulse to give the pronounced kink at the trailing edge of the pulse. The blue curves are biexponential fits with a shared total asymmetry.

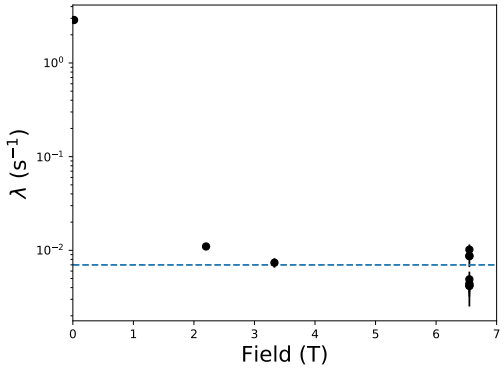

Figure 6. Single exponential spin lattice relaxation rates for ^{8}Li in α-Al_2O_3 at room temperature. The global fit value indicated by the dashed line is 0.0070(3) s^{-1}.

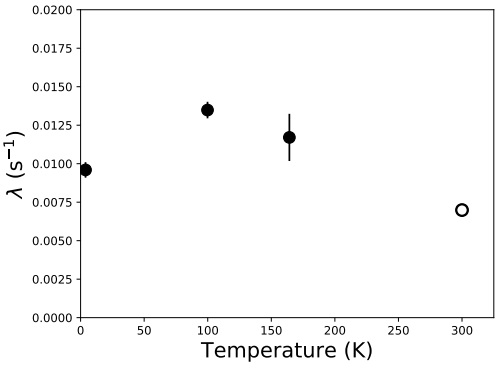

Figure 7. Single exponential spin lattice relaxation rates for ^{8}Li in α-Al_2O_3 at 6.55 Tesla. The open circle is the room temperature global fit value.

5. Spin Lattice Relaxation

While the spin lattice relaxation of ^{8}Li in α-Al_2O_3 is quite fast at low field[7], it is extremely slow at high fields. This is demonstrated in Figure 5 which compares the ^{8}Li relaxation in several materials at 6.55 T and room temperature. The relaxation in sapphire is so slow that it can be used to accurately determine the total experimental asymmetry. This useful calibration allows for identification of a missing fraction such as shown in the magnetic $CrSe_2$[34]. In Figure 5 the relaxation is seen to be considerably faster in rutile TiO_2 and deuterated polystyrene (PS-d8).

In the former case $^8Li^+$ is mobile[35] and the relaxation results from stochastic diffusion. In the latter, glassy dynamics of the host provides analogous fluctuations[36]. In sapphire, neither of these mechanisms is evident.

The relaxation rate is, in fact, so slow that it is difficult to measure due to the lifetime of ^{8}Li. Fitting a single exponential to a set of runs at room temperature that span 15 years, several samples, and a range of fields yields the rates λ shown on a log scale in Figure 6 compared to a similar fit at 200 G. It is clear that the low field relaxation is completely quenched in the interval between 200 G and 2.2 T. This is consistent with a low field relaxation by the ^{27}Al nuclear spins. Unlike the short-lived muon, the host nuclear spins cannot be considered static. This dynamic cross-relaxation is quenched at high fields by the difference in gyromagnetic ratios, and the remnant high field relaxation must have a different origin. For example, there should be slow quadrupolar relaxation from phonons[37] which may be identified by its characteristic power-law temperature dependence (typically T^2 at temperatures comparable to the Debye temperature). However, as seen in Figure 7, the temperature dependence at 6.55 T increases at lower temperatures (in contrast to, e.g., $LaAlO_3$[38]) with some resemblance to the low field temperature dependence[7]. However, the change is not large, and given the magnitude of λ, a more appropriate characterization is merely that λ remains very small down to low temperature. Note that if a paramagnetic defect complex accounts for the missing second site in the spectrum, it is evidently not associated with a distinct faster relaxing signal.

6. Summary

In the high magnetic field βNMR spectra we find evidence of a single crystallographic site for the implanted $^8Li^+$ with an EFG near 63 kHz. Comparison with DFT calculations leads us to conclude that the most likely site is the ideal octahedral interstitial with some relaxation of the surrounding lattice. This case demonstrates that DFT can play an important role improving the interpetation of βNMR measurements and enhancing its use as a probe of materials. Here, it provides critical information on the site of the implanted $^8Li^+$ obtained in a manner complementary to emission channeling[39]. We do not observe a second site that we previously reported based on zero field βNQR. In contrast to low field, the high field spin lattice relaxation is very slow and remains slow down to 4 K.

7. Acknowledgments

We thank Q. Song, D. Wang and D.J. Arseneau for help with the measurements and TRIUMF CMMS and ISAC facility for technical support. J.K. Shenton was supported by the CCP for NMR Crystallography, funded by the Engineering and Physical Sciences Research Council under Grant No. EP/T026642/1.

References

[1] Kumaran R, Webster S E, Penson S, Li W, Tiedje T, Wei P and Schiettekatte F 2009 *Opt. Lett.* **34** 3358–3360 URL http://www.osapublishing.org/ol/abstract.cfm?URI=ol-34-21-3358
[2] Levy P W 1961 *Phys. Rev.* **123**(4) 1226–1233 URL https://link.aps.org/doi/10.1103/PhysRev.123.1226
[3] Evans B D, Pogatshnik G J and Chen Y 1994 *Nuclear Instruments and Methods in Physics Research Section B: Beam Interactions with Materials and Atoms* **91** 258–262 ISSN 0168-583X URL https://www.sciencedirect.com/science/article/pii/0168583X94962278
[4] Yukihara E G and McKeever S W S 2008 *Physics in Medicine and Biology* **53** R351–R379 URL https://doi.org/10.1088/0031-9155/53/20/r01
[5] Al Ghamdi A and Townsend P 1990 *Nuclear Instruments and Methods in Physics Research Section B: Beam Interactions with Materials and Atoms* **46** 133–136 ISSN 0168-583X URL https://www.sciencedirect.com/science/article/pii/0168583X9090684M
[6] Seitbayev A, Skuratov V, Dauletbekova A, Teterev Y, Krylov A, Mamatova M, Koloberdin M and Zdorovets M 2021 *Nuclear Instruments and Methods in Physics Research Section B: Beam Interactions with Materials*

and Atoms **500-501** 46–51 ISSN 0168-583X URL https://www.sciencedirect.com/science/article/pii/S0168583X21001737

[7] Salman Z, Chow K H, Hossain M D, Kiefl R F, Levy C D P, Parolin T J, Pearson M R, Saadaoui H, Wang D and MacFarlane W A 2014 *J. Phys.: Conf. Ser.* **551** 012034 URL http://stacks.iop.org/1742-6596/551/i=1/a=012034

[8] Woodruff D P 2013 *Chemical Reviews* **113** 3863–3886 URL https://doi.org/10.1021/cr3002998

[9] Cortie D L, Buck T, Dehn M H, Karner V L, Kiefl R F, Levy C D P, McFadden R M L, Morris G D, McKenzie I, Pearson M R, Wang X L and MacFarlane W A 2016 *Phys. Rev. Lett.* **116**(10) 106103 URL http://link.aps.org/doi/10.1103/PhysRevLett.116.106103

[10] Cohen M H and Reif F 1957 *Solid State Physics* **5** 321 – 438 ISSN 0081-1947

[11] Abragam A 1983 The international series of monographs on physics, vol 32 (Oxford University Press) ISBN 9780198520146

[12] Dehn M H, Shenton J K, Holenstein S, Meier Q N, Arseneau D J, Cortie D L, Hitti B, Fang A C Y, MacFarlane W A, McFadden R M L, Morris G D, Salman Z, Luetkens H, Spaldin N A, Fechner M and Kiefl R F 2020 *Phys. Rev. X* **10**(1) 011036 URL https://link.aps.org/doi/10.1103/PhysRevX.10.011036

[13] Clark S J, Segall M D, Pickard C J, Hasnip P J, Probert M I J, Refson K and Payne M C 2005 *Zeitschrift für Kristallographie - Crystalline Materials* **220** 567–570 ISSN 2196-7105

[14] Profeta M, Mauri F and Pickard C J 2003 *Journal of the American Chemical Society* **125** 541–548 ISSN 0002-7863 URL https://doi.org/10.1021/ja027124r

[15] Yates J R, Pickard C J and Mauri F 2007 *Physical Review B* **76** 024401

[16] Perdew J P, Ruzsinszky A, Csonka G I, Vydrov O A, Scuseria G E, Constantin L A, Zhou X and Burke K 2008 *Physical Review Letters* **100** 136406 ISSN 0031-9007 (*Preprint* 0707.2088)

[17] Pillet S, Souhassou M, Lecomte C, Schwarz K, Blaha P, Rérat M, Lichanot A and Roversi P 2001 *Acta Crystallographica Section A: Foundations of Crystallography* **57** 290–303 ISSN 0108-7673

[18] Woo A 1999 *Bulletin of the Korean Chemical Society* **20** 1205–1208 URL https://www.koreascience.or.kr/article/JAKO199913464469862.page

[19] MacFarlane W, Shenton J, Salman Z, Chatzichristos A, Cortie D, Dehn M, Fujimoto D, Karner V, Kiefl R, Koumoulis D, Levy C, McFadden R, McKenzie I, Morris G, Pearson M, Stachura M and Ticknor J 2022 The $^{8}Li^{+}$ site in α-Al_2O_3: supplemental material (v1.0) https://doi.org/10.5281/zenodo.7030274

[20] Cortie D L, Buck T, Dehn M H, Kiefl R F, Levy C D P, McFadden R M L, Morris G D, Pearson M R, Salman Z, Maeno Y and MacFarlane W A 2015 *Phys. Rev. B* **91**(24) 241113 URL http://link.aps.org/doi/10.1103/PhysRevB.91.241113

[21] Adelman J R, Fujimoto D, Dehn M H, Dunsiger S R, Karner V L, Levy C D P, Li R, McKenzie I, McFadden R M L, Morris G D, Pearson M R, Stachura M, Thoeng E, Ticknor J O, Ohashi N, Kojima K M and MacFarlane W A 2022 *Phys. Rev. B* **106**(3) 035205 URL https://link.aps.org/doi/10.1103/PhysRevB.106.035205

[22] Salman Z, Reynard E P, MacFarlane W A, Chow K H, Chakhalian J, Kreitzman S R, Daviel S, Levy C D P, Poutissou R and Kiefl R F 2004 *Phys. Rev. B* **70**(10) 104404 URL http://link.aps.org/doi/10.1103/PhysRevB.70.104404

[23] Karner V L, McFadden R M L, Dehn M H, Fujimoto D, Chatzichristos A, Morris G D, Pearson M R, Levy C D P, Reisner A, Tjeng L H, Kiefl R F and MacFarlane W A 2018 *JPS Conf. Proc.* **21** 011024 (*Preprint* https://journals.jps.jp/doi/pdf/10.7566/JPSCP.21.011024) URL https://journals.jps.jp/doi/abs/10.7566/JPSCP.21.011024

[24] Nikolaev A V, Chtchelkatchev N M, Salamatin D A and Tsvyashchenko A V 2020 *Phys. Rev. B* **101**(6) 064310 URL https://link.aps.org/doi/10.1103/PhysRevB.101.064310

[25] MacFarlane W A, Tschense C B L, Buck T, Chow K H, Cortie D L, Hariwal A N, Kiefl R F, Koumoulis D, Levy C D P, McKenzie I, McGee F H, Morris G D, Pearson M R, Song Q, Wang D, Hor Y S and Cava R J 2014 *Phys. Rev. B* **90**(21) 214422 URL http://link.aps.org/doi/10.1103/PhysRevB.90.214422

[26] Jacobs P W M and Kotomin E A 1994 *Journal of the American Ceramic Society* **77** 2505–2508 (*Preprint* https://ceramics.onlinelibrary.wiley.com/doi/pdf/10.1111/j.1151-2916.1994.tb04635.x) URL https://ceramics.onlinelibrary.wiley.com/doi/abs/10.1111/j.1151-2916.1994.tb04635.x

[27] Zhang H, Zhang M, Hu Z, Han J, Guo H and Xu C 2012 *Nuclear Instruments and Methods in Physics Research Section B: Beam Interactions with Materials and Atoms* **291** 73–76 ISSN 0168-583X URL https://www.sciencedirect.com/science/article/pii/S0168583X12005976

[28] Tsunoda N, Kumagai Y and Oba F 2022 *Computational Materials Science* **203** 111068 ISSN 0927-0256 URL https://www.sciencedirect.com/science/article/pii/S0927025621007436

[29] Alves E, da Silva M, van den Hoven G, Polman A, Melo A and Soares J 1995 *Nuclear Instruments and Methods in Physics Research Section B: Beam Interactions with Materials and Atoms* **106** 429–432 ISSN

0168-583X ion Beam Modification of Materials URL https://www.sciencedirect.com/science/article/pii/0168583X95007466

[30] Shannon R D 1976 *Acta Crystallographica Section A* **32** 751–767 URL https://doi.org/10.1107/S0567739476001551

[31] Möller J S, Ceresoli D, Lancaster T, Marzari N and Blundell S J 2013 *Phys. Rev. B* **87**(12) 121108 URL https://link.aps.org/doi/10.1103/PhysRevB.87.121108

[32] Ashbrook S E and McKay D 2016 *Chem. Commun.* **52**(45) 7186–7204 URL http://dx.doi.org/10.1039/C6CC02542K

[33] Kotomin E and Popov A 1998 *Nuclear Instruments and Methods in Physics Research Section B: Beam Interactions with Materials and Atoms* **141** 1–15 ISSN 0168-583X URL https://www.sciencedirect.com/science/article/pii/S0168583X98000792

[34] Ticknor J O, Umegaki I, McFadden R M L, Chatzichristos A, Fujimoto D, Karner V L, Kiefl R F, Kobayashi S, Levy C D P, Li R, Morris G D, Pearson M R, Yoshimura K, Sugiyama J and MacFarlane W A 2020 *RSC Adv.* **10**(14) 8190–8197 URL http://dx.doi.org/10.1039/C9RA07065F

[35] McFadden R M L, Buck T J, Chatzichristos A, Chen C C, Chow K H, Cortie D L, Dehn M H, Karner V L, Koumoulis D, Levy C D P, Li C, McKenzie I, Merkle R, Morris G D, Pearson M R, Salman Z, Samuelis D, Stachura M, Xiao J, Maier J, Kiefl R F and MacFarlane W A 2017 *Chemistry of Materials* **29** 10187–10197 URL https://doi.org/10.1021/acs.chemmater.7b04093

[36] McKenzie I, Chai Y, Cortie D L, Forrest J A, Fujimoto D, Karner V L, Kiefl R F, Levy C D P, MacFarlane W A, McFadden R M L, Morris G D, Pearson M R and Zhu S 2018 *Soft Matter* **14** 7324–7334 URL http://dx.doi.org/10.1039/C8SM00812D

[37] Van Kranendonk J and Walker M B 1968 *Canadian Journal of Physics* **46** 2441–2461 URL https://doi.org/10.1139/p68-604

[38] Karner V L, McFadden R M L, Chatzichristos A, Morris G D, Pearson M R, Levy C D P, Salman Z, Cortie D L, Kiefl R F and MacFarlane W A 2018 *JPS Conf. Proc.* **21** 011023 (*Preprint* https://journals.jps.jp/doi/pdf/10.7566/JPSCP.21.011023) URL https://journals.jps.jp/doi/abs/10.7566/JPSCP.21.011023

[39] Wahl U 1997 *Phys. Rep.* **280** 145 URL http://www.sciencedirect.com/science/article/pii/S037015739600021X